The interactions between the 2018 Lombok earthquake sequence, Indonesia and the unrest Rinjani-Samalas volcanic complex

Siyuan Zhao[1,2], Susanna Ebmeier[1], John Elliott[1], Phil Cummins[2], Milan Lazecky[1] and Pedro Espin Bedon[1]

- [1] COMET, Institute of Geophysics and Tectonics, University of Leeds (S.Zhao@Leeds.ac.uk)
- [2] The Australian National University, Research School of Earth Sciences, Australia

Dawn view from the summit of Gunung Rinjani. rob_travel/Shutterstock

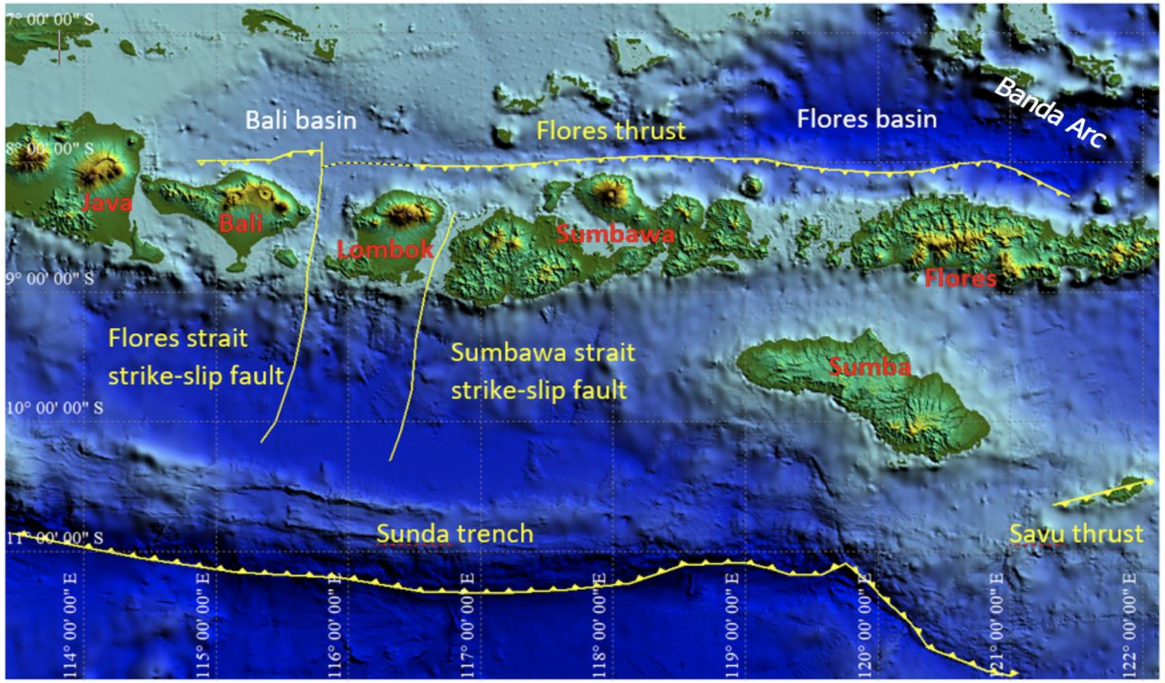

- The island of Lombok is located at the eastern Indonesia, tectonically bounded by Flores back-arc thrust fault and Sunda subduction megathrust.

- The highly active Rinjani volcano is located at the north Lombok Island, which is the second largest volcano in Indonesia.

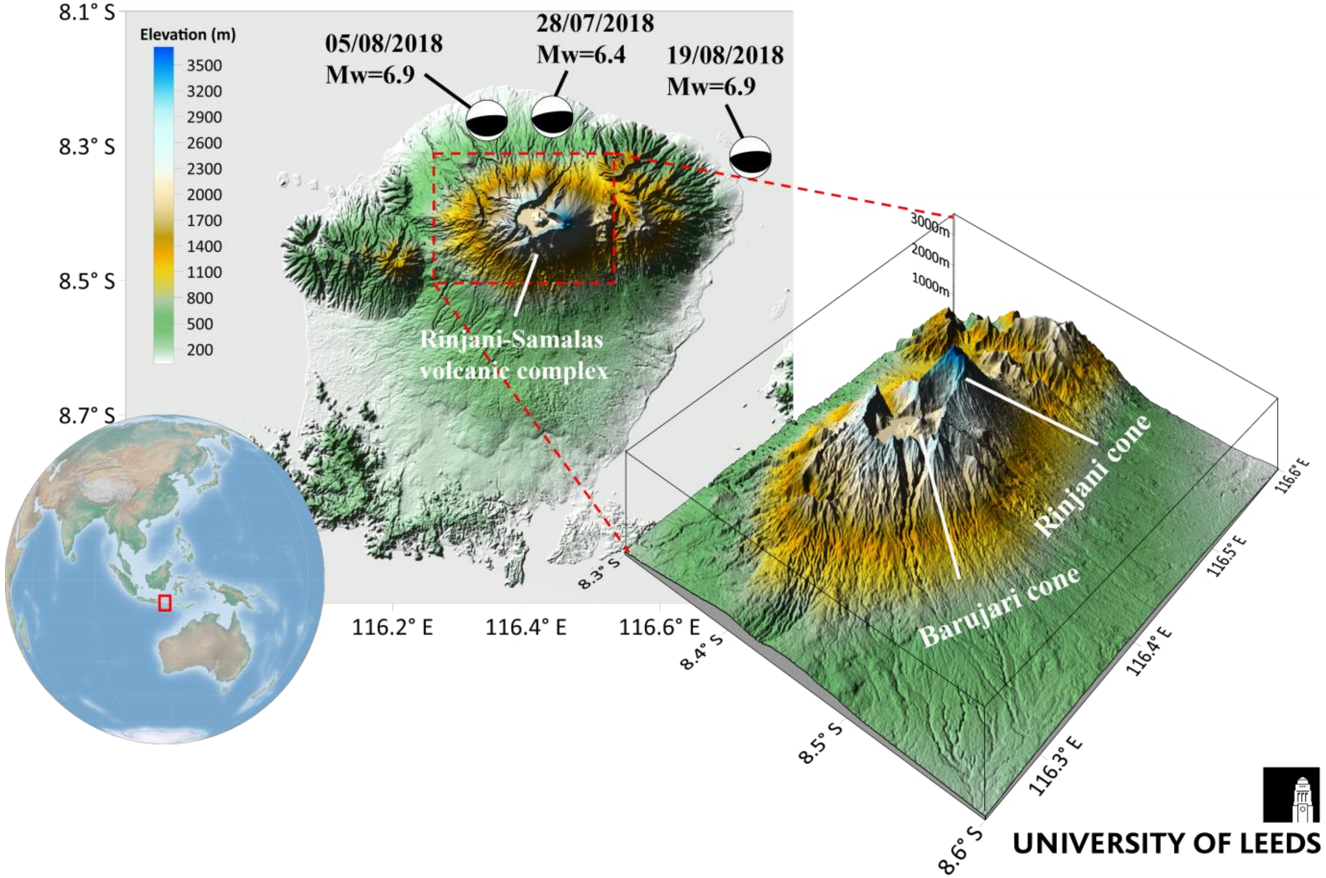

- In 2018, four deadly (Mw 6.2-6.9) earthquakes struck the north coast of Lombok Island.

- The proximity of the earthquake sequence to the volcano, coupled with the stress change, raises the question of how the earthquake sequence influenced the Rinjani volcano's deformation.

UNIVERSITY OF LEEDS

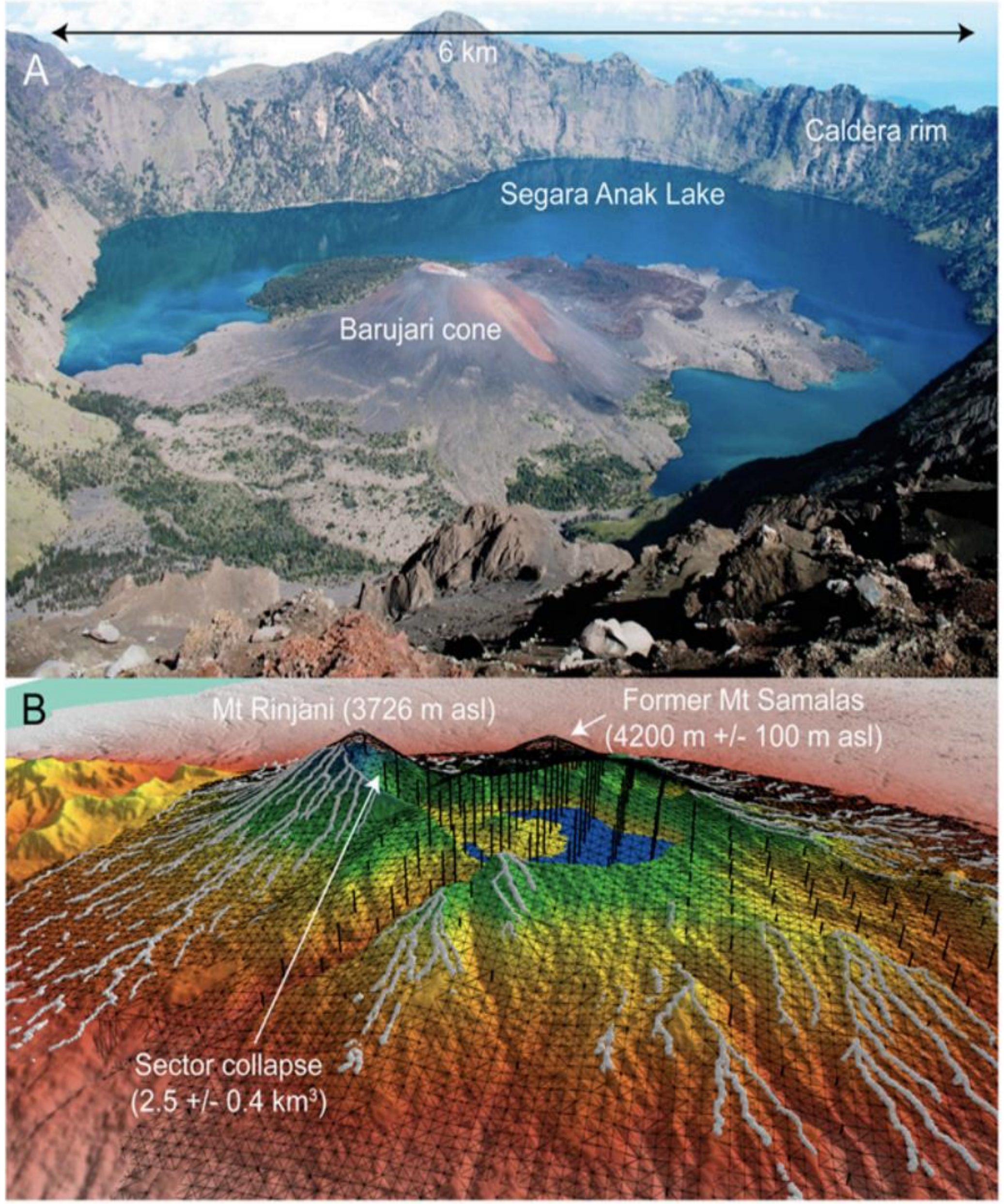

- In 1257, a catastrophic eruption occurred on the former Mt Samalas, leading to the caldera collapse, with volcanic activity shifting to Barujari volcano on the caldera rim (Lavigne et al., 2013).

- The Segara Anak lake filling the caldera of Rinjani volcano, surrounding the Barujari cone. The lake covers an area of 11 km^2, which is one of the largest hot volcanic lakes in the world.

UNIVERSITY OF LEEDS

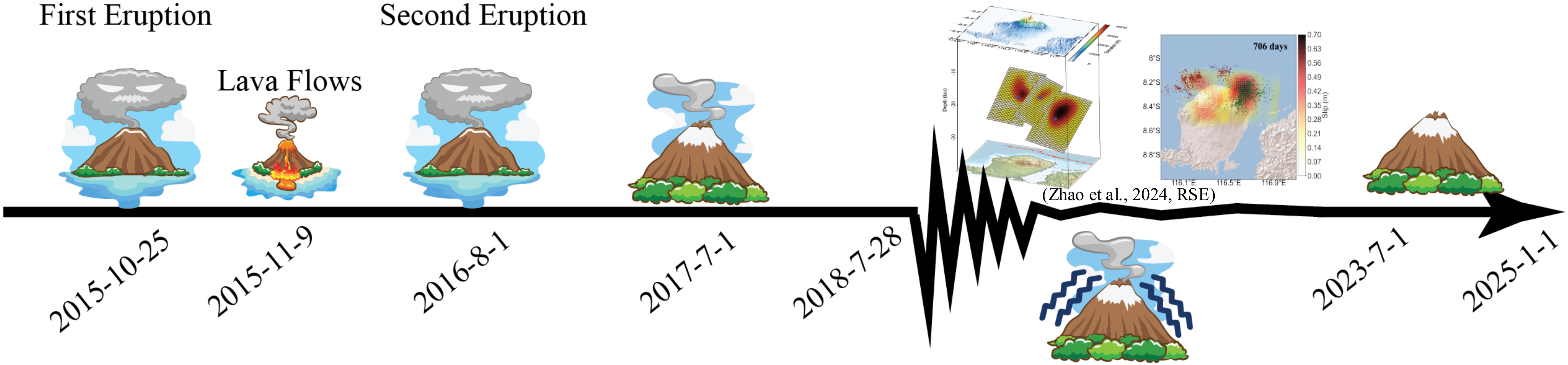

Eruption in 2015

- In 2015, a series of eruptions occurred from 25 October to 24 December with the maximum height of the ash reported to reach up to 6 km, along with pyroclastic and lava flow.

- In 2016, a similar eruption occurred on 1 August, generating a 10 km high ash plume; follow-up small-scale explosive activity occurred in September 2016.

- In 2018, the earthquake sequence occurred, characterised by an irregular shaped seismogeneric fault and long-persisted afterslip (Zhao et al., 2024).

UNIVERSITY OF LEEDS

InSAR Time Series

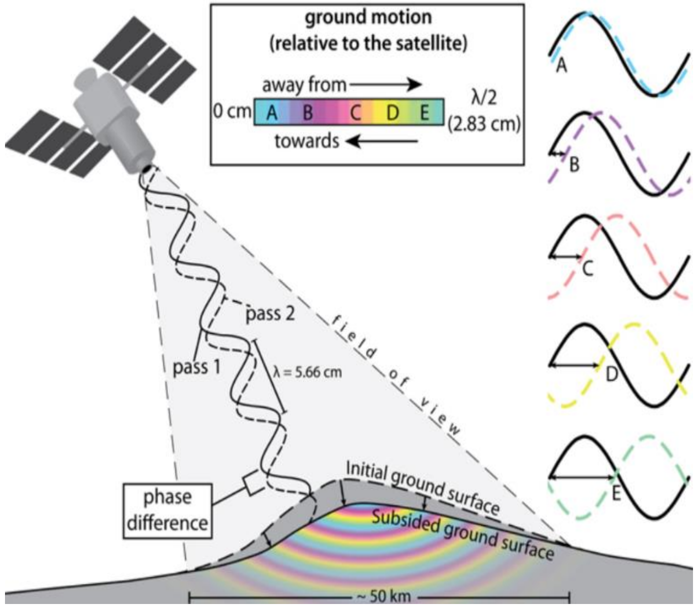

Loa (2012)

- InSAR technology detects the ground deformation based on the phase difference.
- LiCSAR (Lazecký et al., 2020) were used for the interferometric processing of Sentinel-1 data from 2014 to 2025.

- The InSAR interferograms were analysed using LiCSBAS (Morishita et al., 2020), which implements the re-unwrapping (Lazecký et al., 2022) and nullification approaches (Lazecký et al., 2024) .
- In this study, 1215 descending and 1578 ascending Sentinel-1 interferograms are used to build up the time series of the over ten-year's deformation. TanDEM-X high-resolution DEM are used to mitigate the topography effects for caldera region.

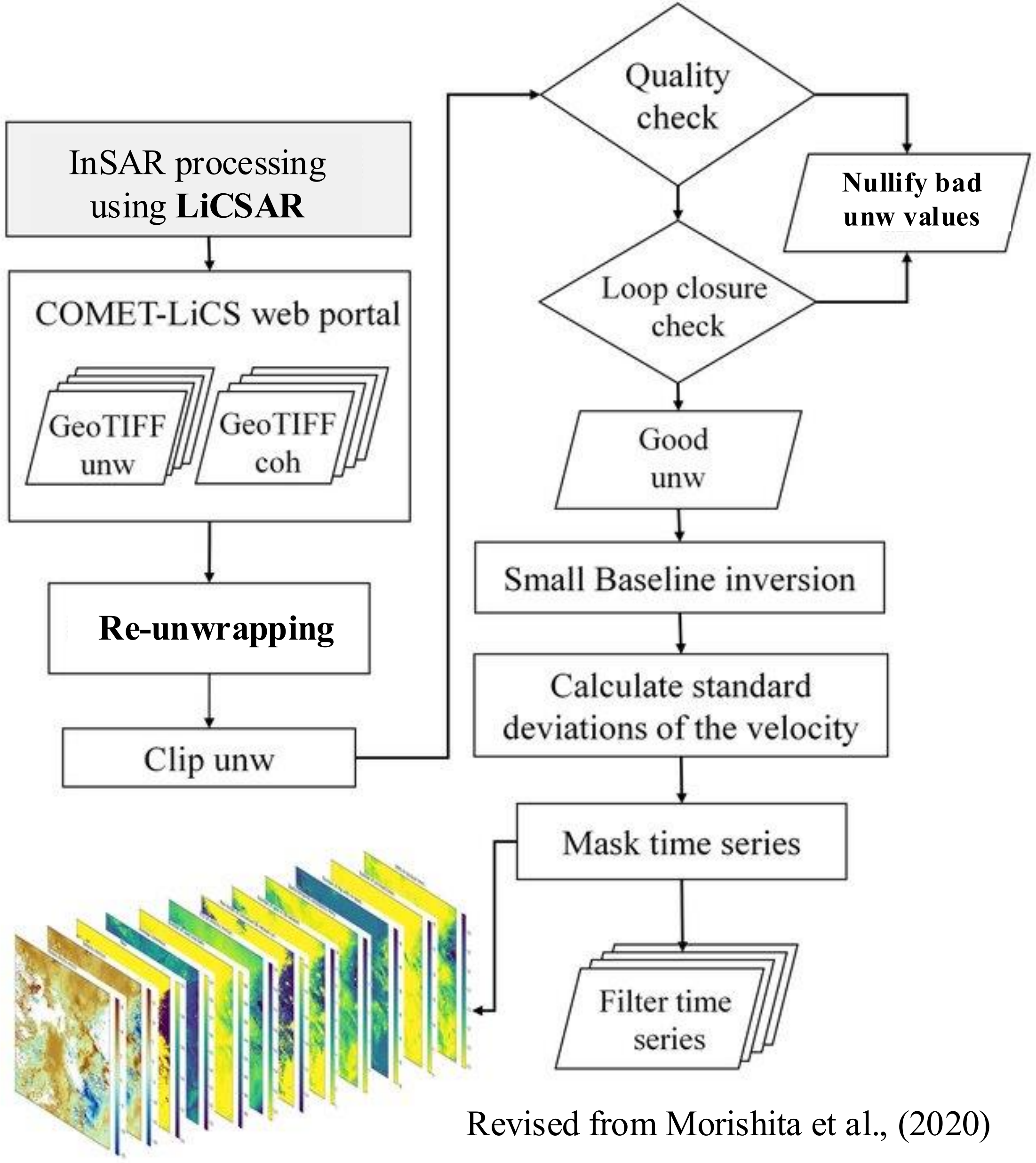

Revised from Morishita et al., (2020)

UNIVERSITY OF LEEDS

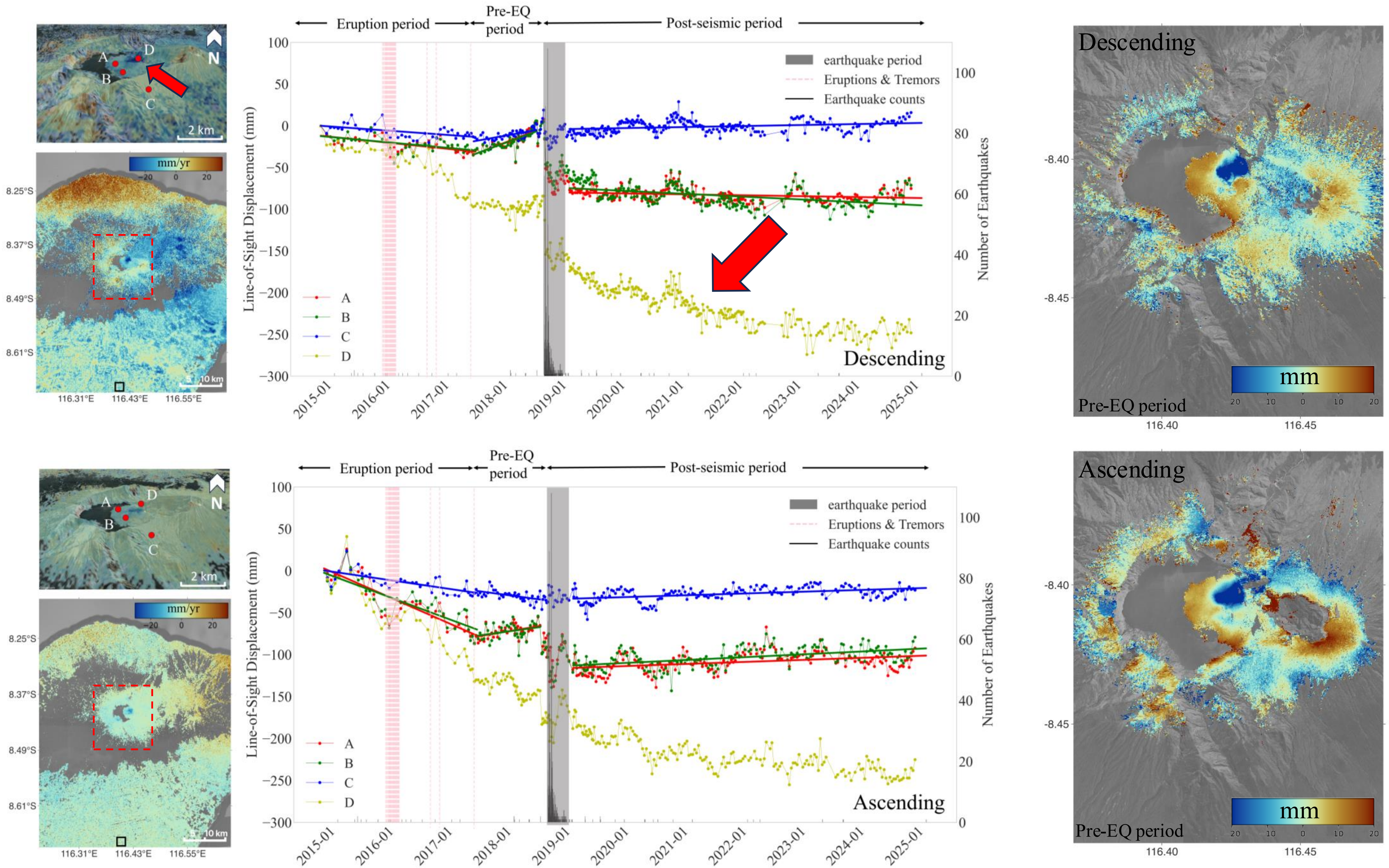

N
A
B
C
D
2 km
mm/yr
−20
0
20
8.25°S
8.37°S
8.49°S
8.61°S
10 km
116.31°E
116.43°E
116.55°E
Eruption period
Pre-EQ period
Post-seismic period
earthquake period
Eruptions & Tremors
Earthquake counts
Line-of-Sight Displacement (mm)
Number of Earthquakes
Descending
Ascending
2015-01
2016-01
2017-01
2018-01
2019-01
2020-01
2021-01
2022-01
2023-01
2024-01
2025-01
mm
Pre-EQ period
-8.40
-8.45
116.40
116.45

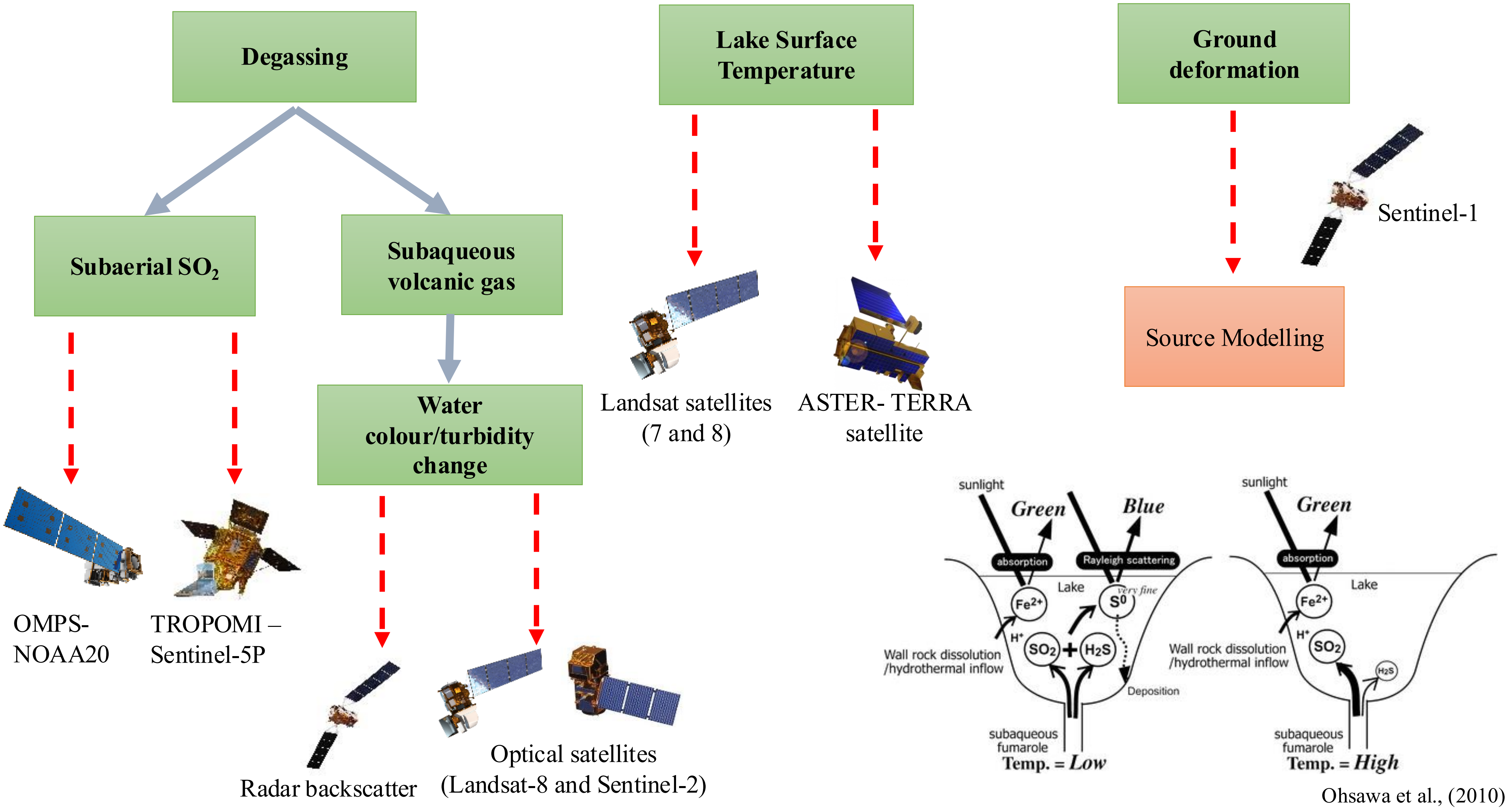
Degassing
Subaerial SO_2
Subaqueous volcanic gas
Water colour/turbidity change
OMPS-NOAA20
TROPOMI – Sentinel-5P
Radar backscatter
Optical satellites (Landsat-8 and Sentinel-2)
Lake Surface Temperature
Landsat satellites (7 and 8)
ASTER- TERRA satellite
Ground deformation
Sentinel-1
Source Modelling
sunlight
Green
Blue
absorption
Rayleigh scattering
Lake
very fine
Fe^{2+}
S^0
H^+
SO_2
H_2S
Wall rock dissolution /hydrothermal inflow
Deposition
subaqueous fumarole
Temp. = Low
Temp. = High
Ohsawa et al., (2010)

Subaerial SO_2

- The SO_2 flux was calculated by integrating the measurements from the Ozone Mapping and Profiler Suite (OMPS) and TROPOspheric Monitoring Instrument (TROPOMI) using the special averaging method (disk method; Grandin et al., 2024).
- In addition to the TROPOMI Level 2 (L2) products, more sensitive TROPOMI-COBRA (Covariance-Based Retrieval Algorithm) products (Fioletov et al., 2023) were employed.
- Data were filtered based on European Centre for Medium-Range Weather Forecasts Reanalysis V5 (ECMWF ERA5) wind azimuths and the SO_2 Vertical Column Density (VCD) is retrieved assuming a plume centre-of-mass at 1 km.

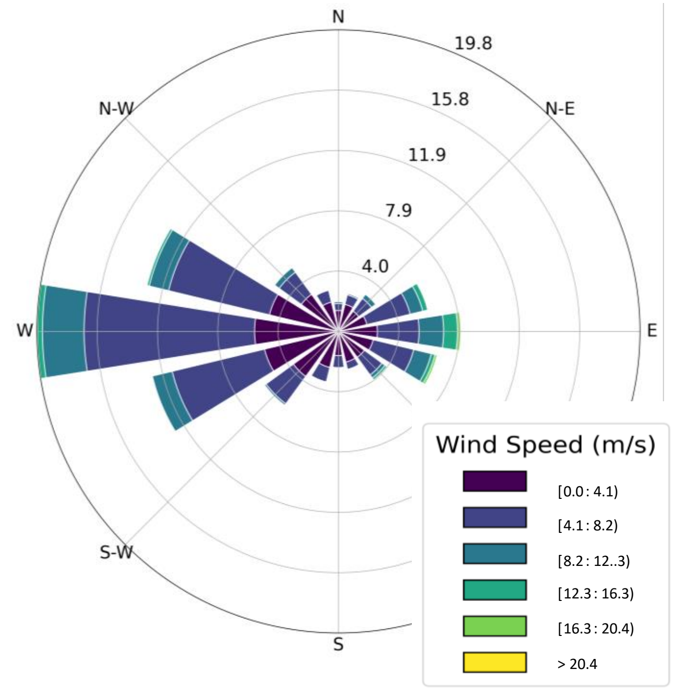

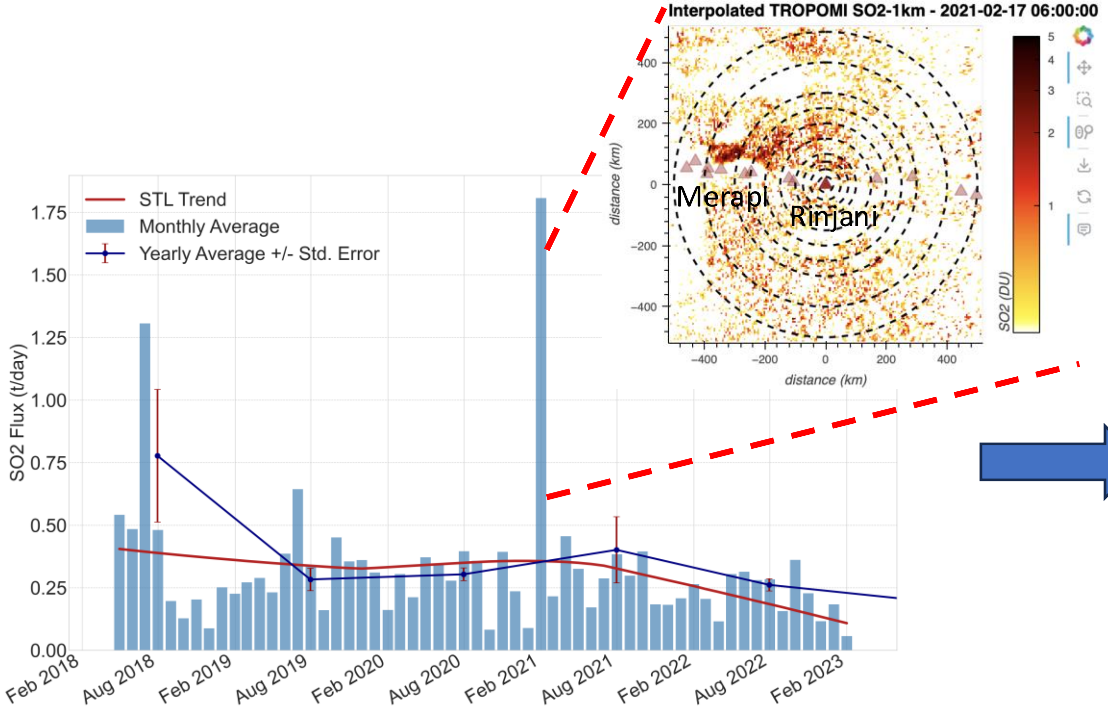

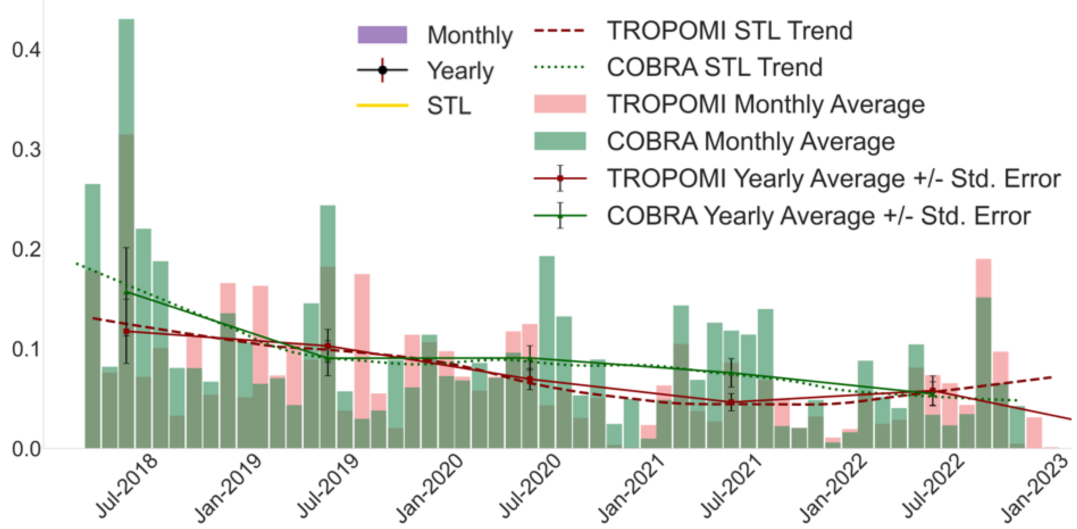

UNIVERSITY OF LEEDS

Subaqueous volcanic gas

--Lake colour/turbidity remote sensing

Forel-Ule Index

The FUI is an index for describing the colour of a body of water, which is calculated from satellite reflectance according to the band settings of different spectrometers.

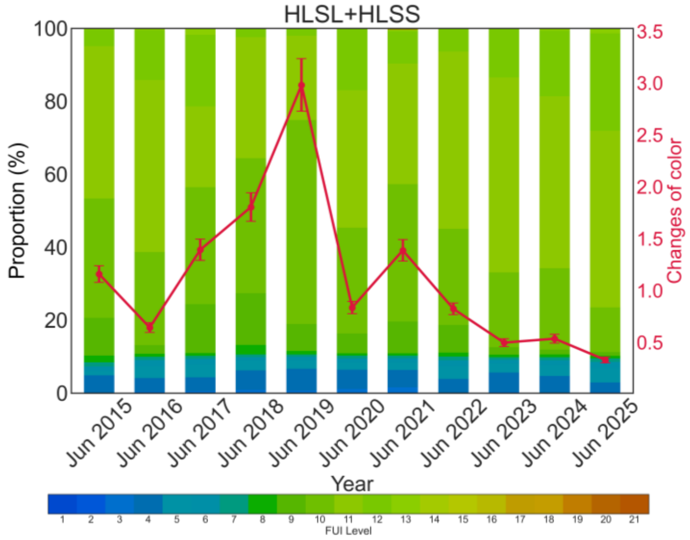

HLS Products: These are processed data products created by the Harmonized Landsat Sentinel-2 project, which aims to provide consistent land surface information from both Landsat and Sentinel-2 satellites (Ju et al., 2025).

2014 2017 2018 2024

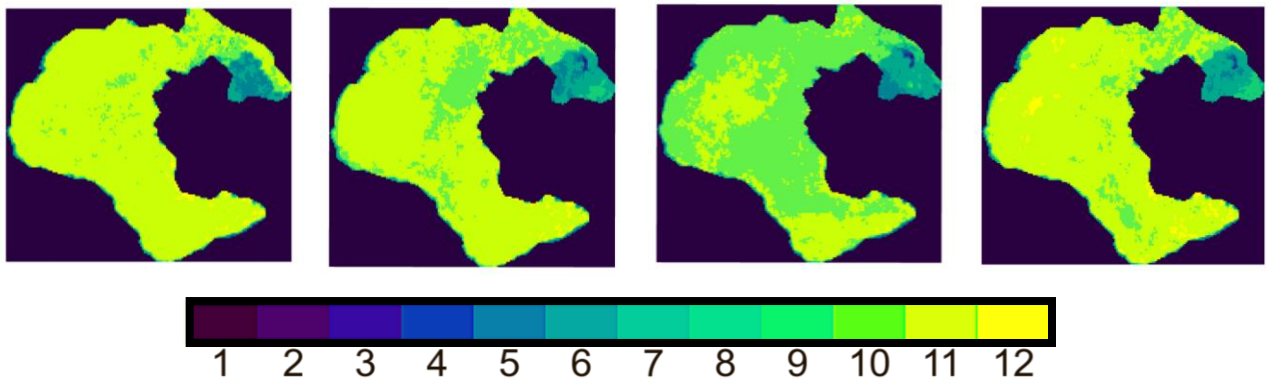

Modified Forel-Ule Index (FUI) value

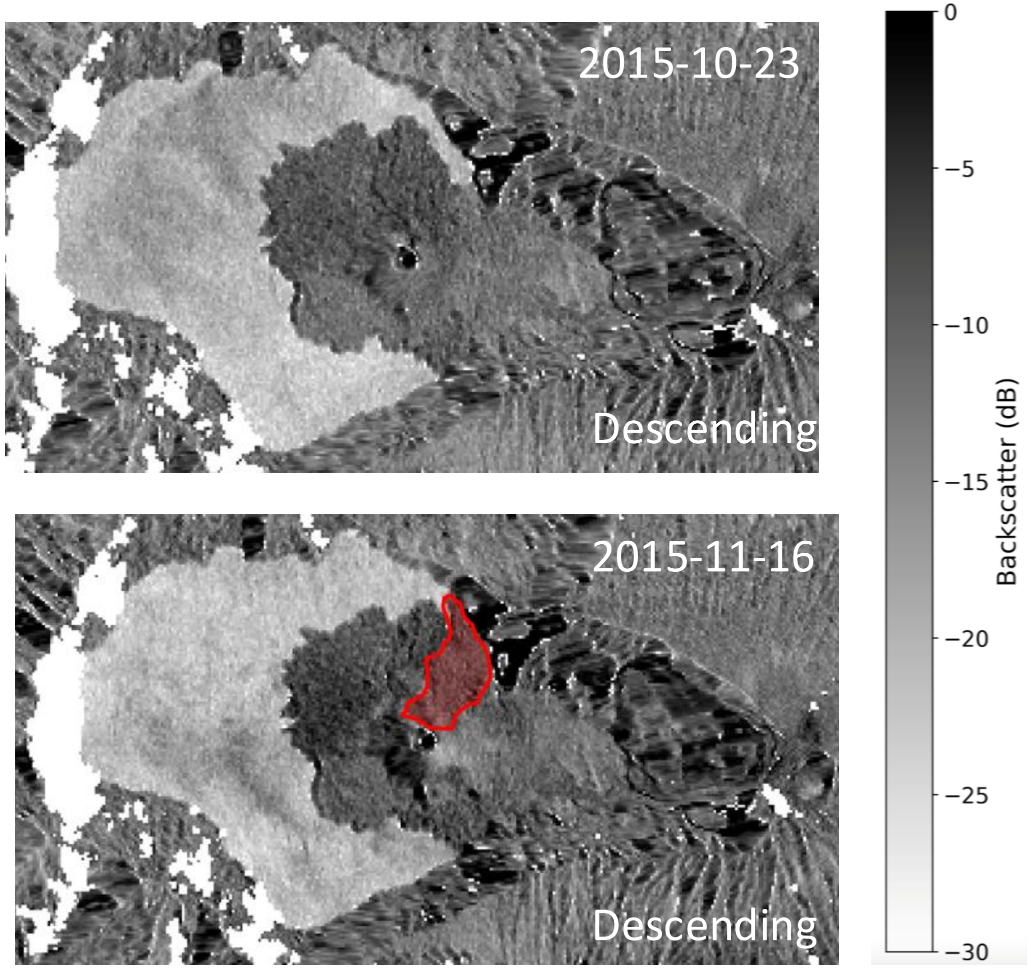

Cloud-independent SAR backscatter were used to analyse the turbidity changes caused by colloidal sulphur particles, comparing with lake colour changes derived from optical satellite time series.

UNIVERSITY OF LEEDS

Source Modelling

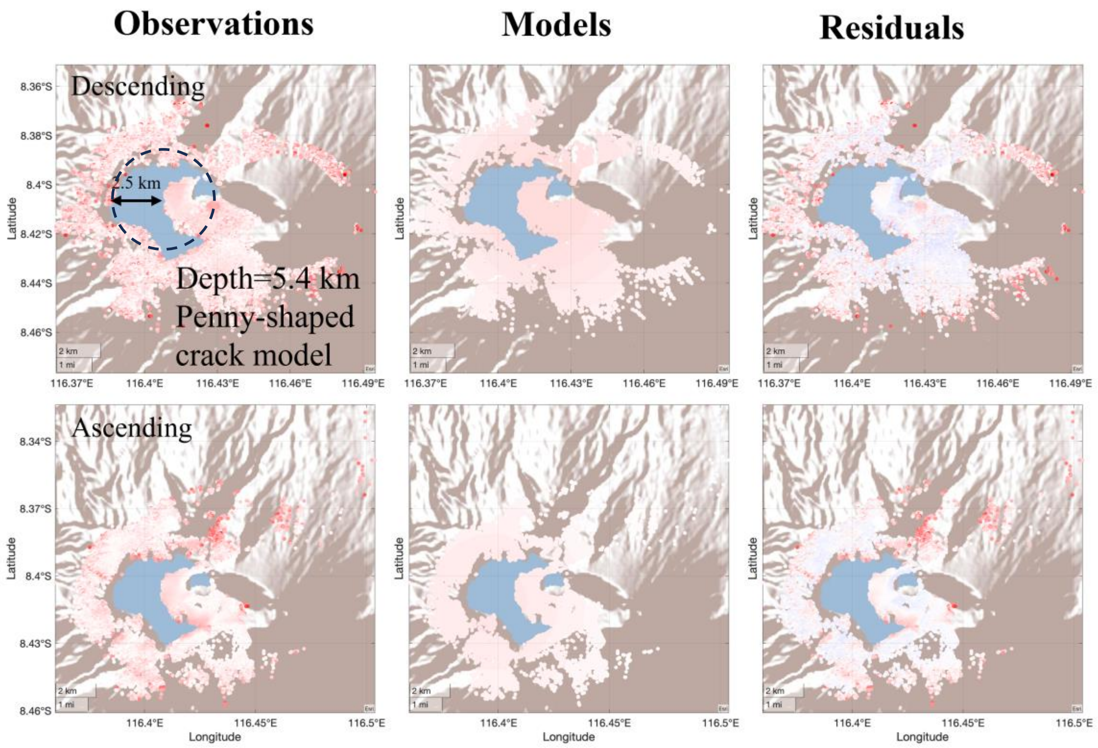

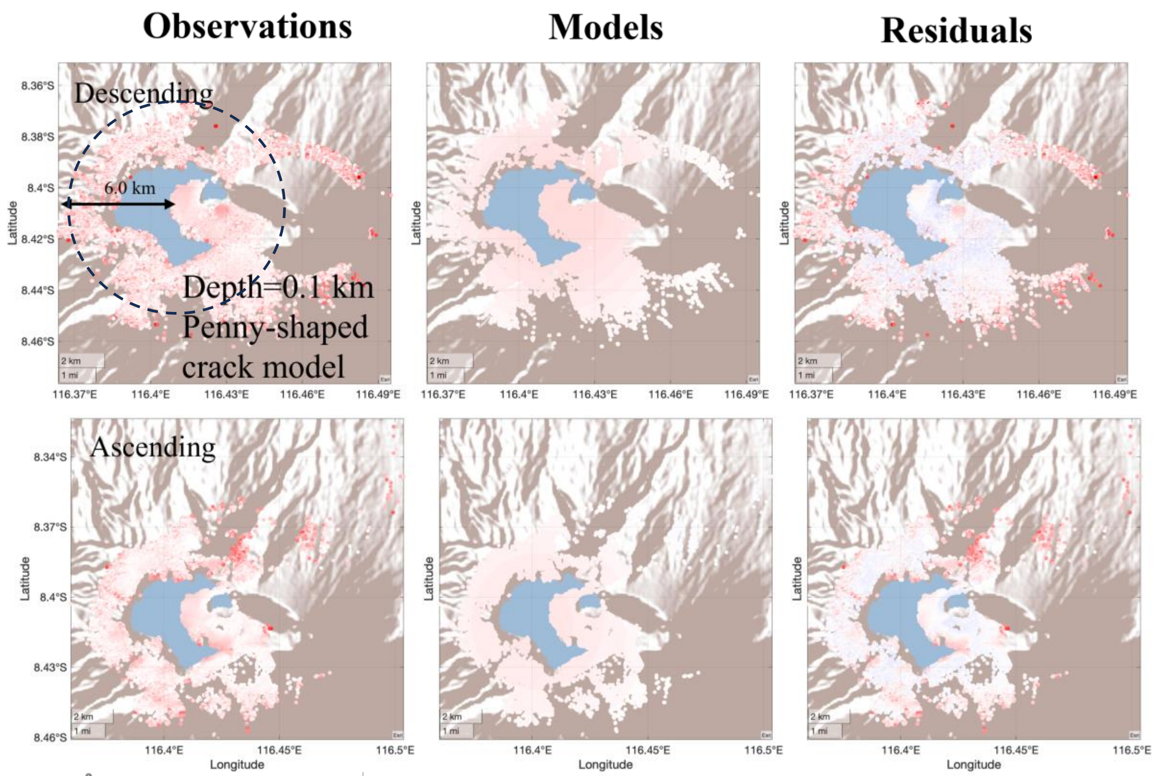

- Penny-shaped sill-like source models.
- Two fixed-radius scenarios of 2.5 km and 6.0 km were tested, representing the approximate spatial extents of the caldera lake and the broader volcanic edifice, respectively.
- We performed grid searches algorithm to solve for a coarse depth solution, and inverted for the dimensionless excess pressure changes ($\Delta P/\mu$).

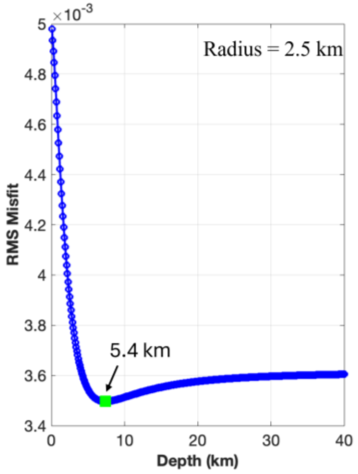

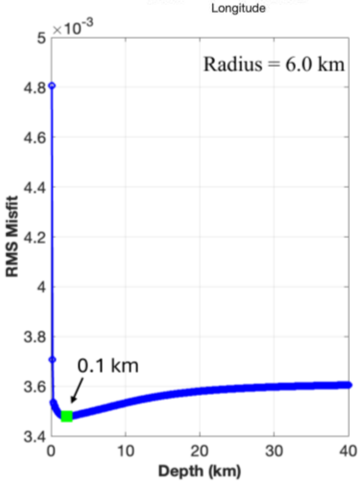

- Optimal depth for a compact 2.5 km radius source was found to be 5.4 km, whereas the optimal depth ascends to 0.1 km when the radius was expanded to 6.0 km, roughly equivalent to the bathymetric depth of the crater lake.
- If the shallow hydrothermal system is a primary volumetric driver, it should extend beyond the boundaries of Segara Anak Lake (radius > 2.5 km).

UNIVERSITY OF LEEDS

Impact of the earthquake sequence on the magmatic and hydrothermal systems

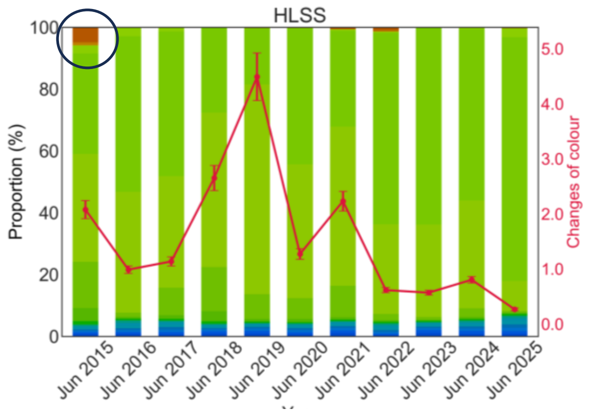

- Subsidence of the volcanic edifice.
- A rapid increase in SO_2 flux following the eruption.
- A steady increase in lake temperature, which peaked in 2016.
- Lake water turbidity reaches its peak during the eruption period.
- Red hue of the lake FUI can be observed in 2015.

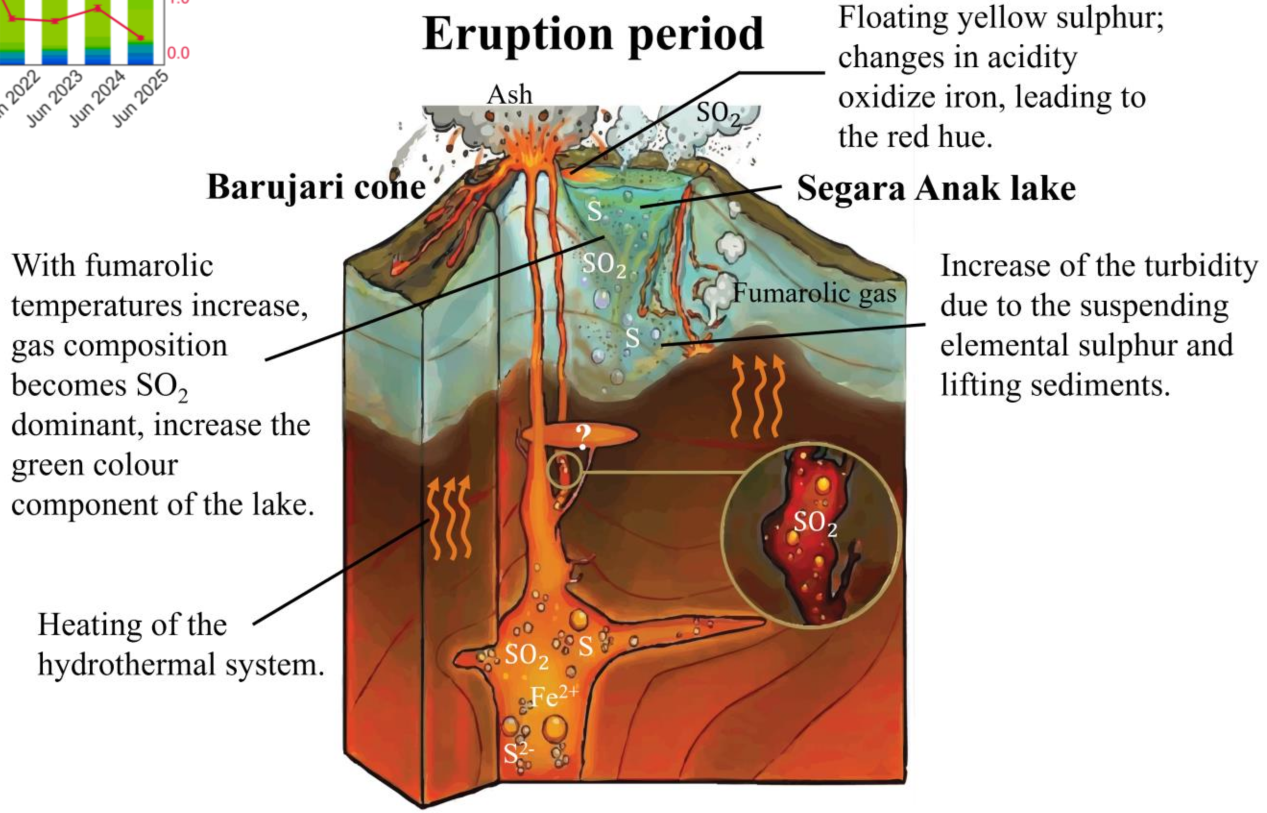

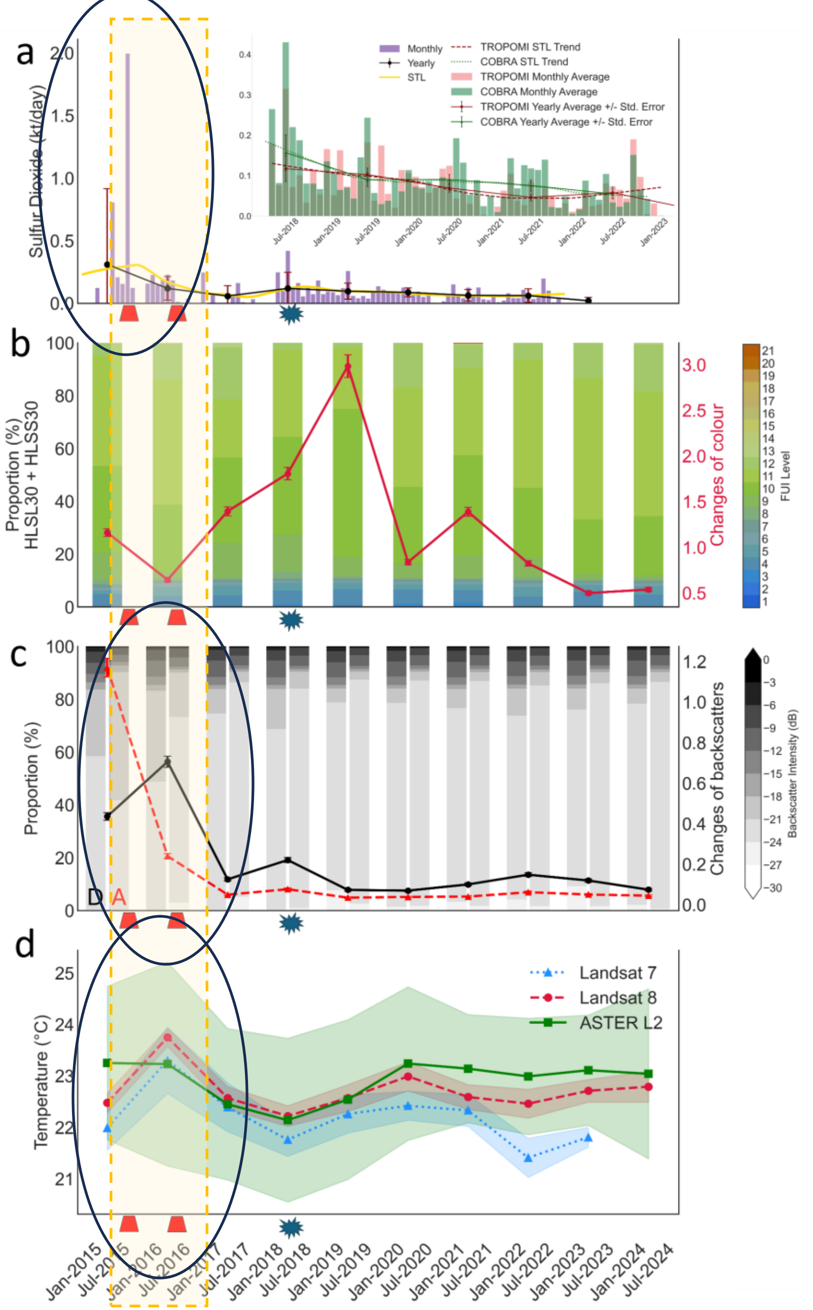

Impact of the earthquake sequence on the magmatic and hydrothermal systems

- Uplift of the caldera region.
- SO_2 emissions increase until the earthquake occurred.
- Lake colour changes, showing an increase in blue-related hue.
- A substantial decline in lake temperature and turbidity.

Pre-seismic/post-eruption period

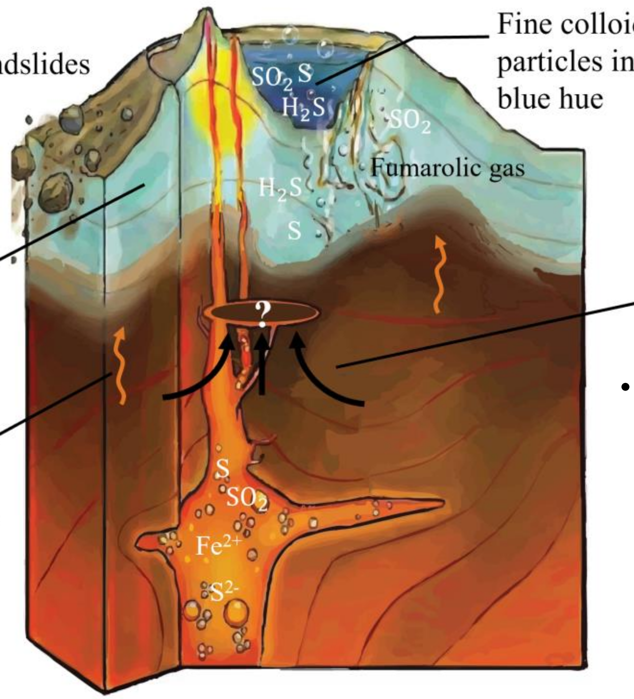

- Calming sediments decrease the turbidity.
- Colloidal sulphur particles increase the turbidity.

- When prior eruptions fail to adequately release pore pressure within the hydrothermal system, shallow inflation can persist continuously during the post-eruption period.

- The inflation was restricted solely to the caldera region and coincided with a significant decrease in lake temperature, implying that the deformation was predominantly driven by the shallower hydrothermal system rather than direct magma chamber recharge.

- Inward flow from the bottom and sides pushes against this rigid elastic lid, contributing to surface uplift

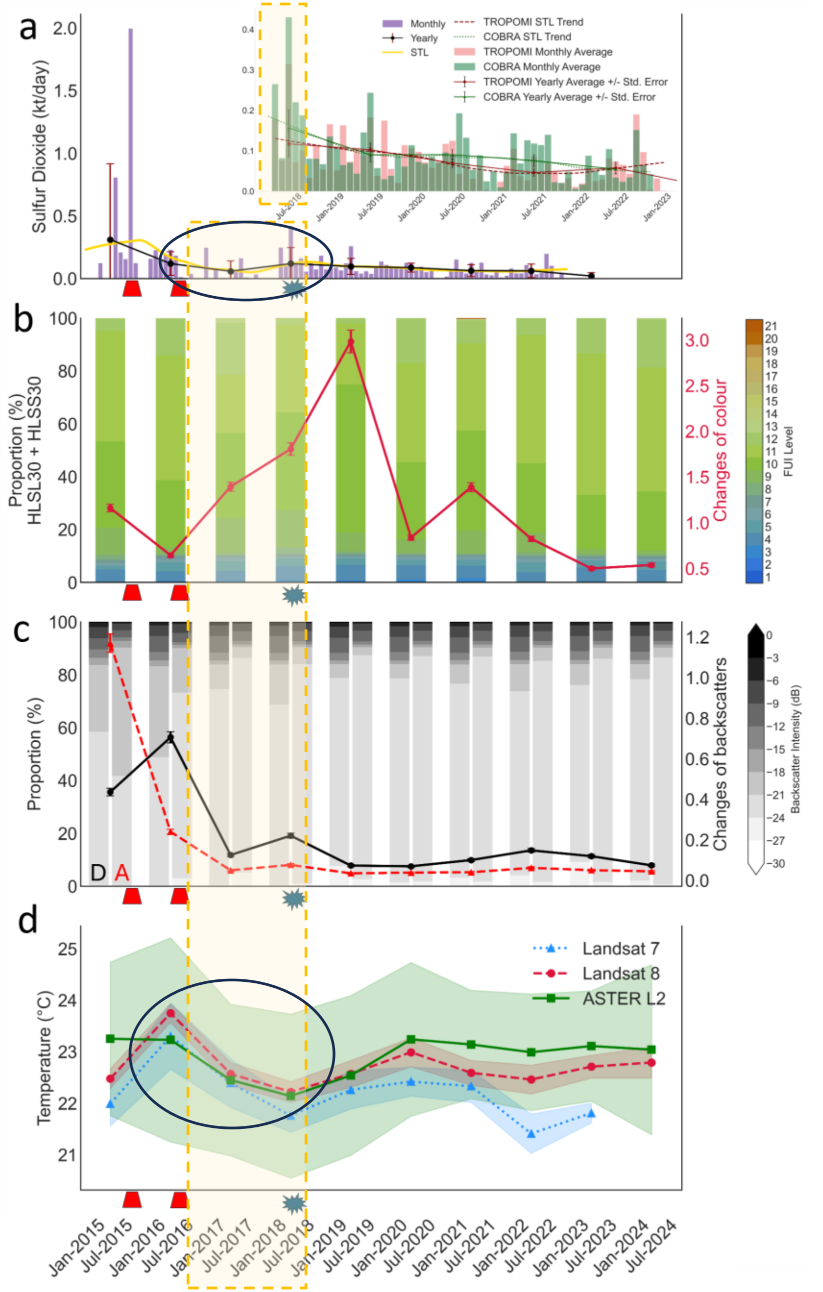

Impact of the earthquake sequence on the magmatic and hydrothermal systems

- Ground deformation became subtle.
- SO_2 emissions show a substantial decrease.
- Lake colour return to the pre-eruption baseline green.
- Land surface temperature and turbidity rose until 2020, and then stabilized.

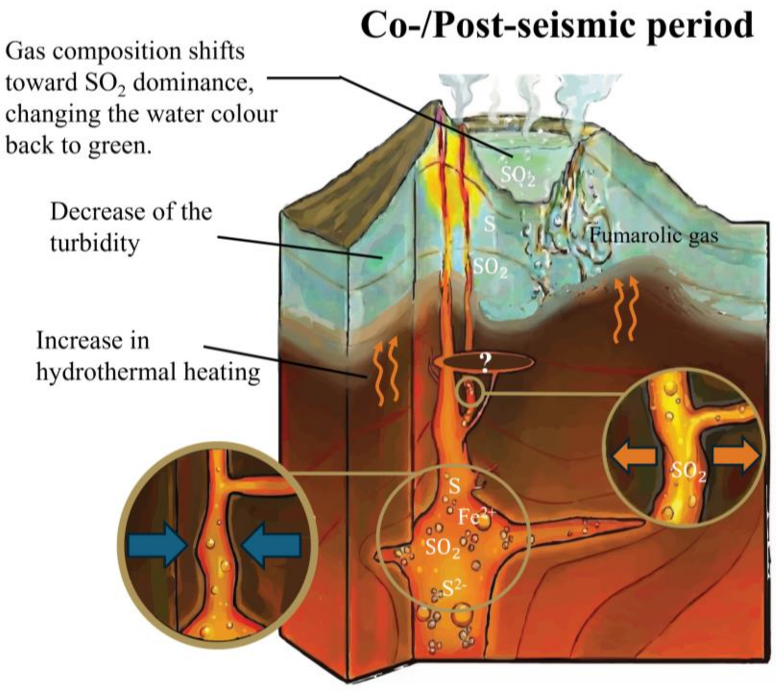

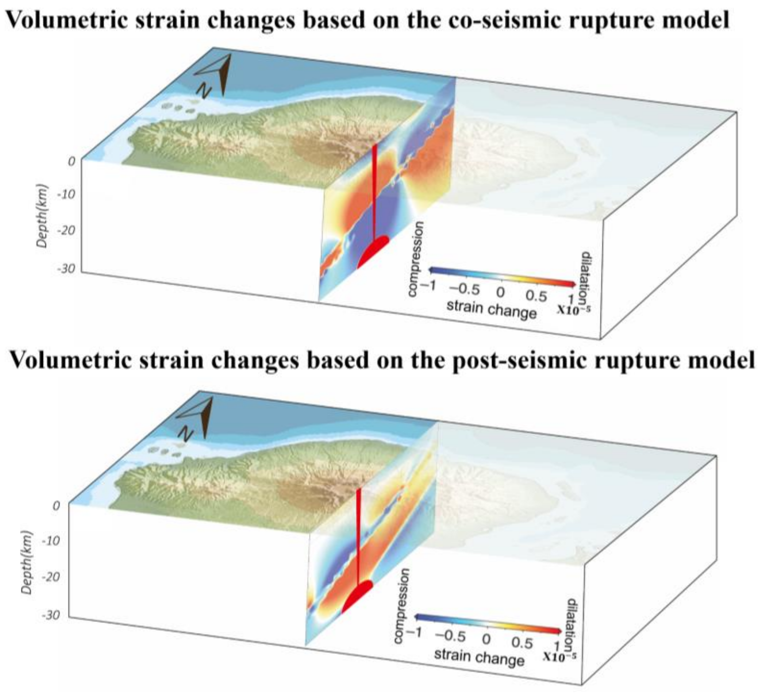

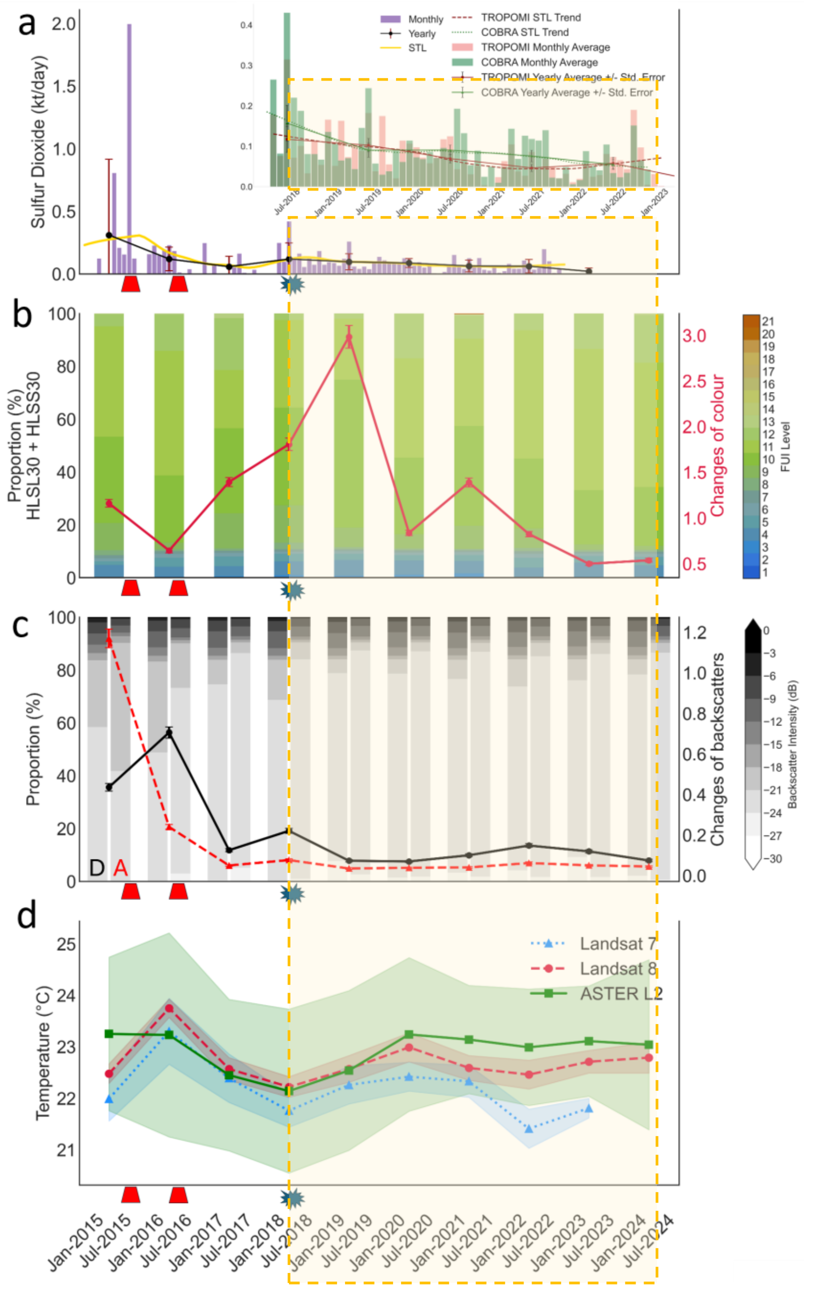

The earthquake-induced fracturing increased the permeability of the edifice, allowing deeply sourced magmatic heat and SO_2-rich fluids to continuously vent into the lake, maintaining high thermal flux while preventing the buildup of mechanical strain.

Take home messages:

Stages			Interpretations
Eruption period (before Jul 2017)	Pre-/Co-EQ period (Jul 2017~Aug 2018)	Post-seismic period (After Aug 2018)	• The earthquake-induced decrease in hydrothermal pore pressure would generally trigger surface subsidence directly above it and cease the ongoing uplift, independent of magmatic movement. • The earthquakes may have also generated shallow open cracks that relieved internal pressure. These strain changes temporarily enhanced degassing, aligning with our time series data showing subaerial SO_2 and the blue hue area peaking in July 2018. • Rather than triggering a volcanic eruption, the 2018 tectonic earthquakes ceased the mechanical inflation. • Earthquake-induced crustal fracturing significantly enhanced the vertical permeability of the volcanic edifice. This fracturing effectively releases trapped magmatic-hydrothermal overpressure while facilitating continuous, efficient advective heat transfer to the surface.
• Subsidence of the volcanic edifice. • A rapid increase in SO_2 flux following the eruption, then a substantial decline. • A steady increase in lake temperature, which peaked in 2016. • A notable decrease in lake water clarity. • Red hue of the lake FUI can be observed in 2015.	• Uplift of the caldera region. • SO_2 emissions increase until the earthquake occurred (July-2018) • Lake colour changes, showing an increase in blue-related hue. • A substantial decline in lake temperature and clarity.	• Ground deformation became subtle. • SO_2 emissions show a substantial decrease. • Lake colour return to the pre-eruption baseline green. • Land surface temperature and clarity rose until 2020, and then stabilized.	

UNIVERSITY OF LEEDS

References:

1. Zhao, S., McClusky, S., Cummins, P. R., & Miller, M. S. (2024). Co-seismic and post-seismic deformation associated with the 2018 Lombok, Indonesia, earthquake sequence, inferred from InSAR and seismic data analysis. Remote Sensing of Environment, 304, 114063.
2. Lavigne, F., Degeai, J. P., Komorowski, J. C., Guillet, S., Robert, V., Lahitte, P., ... & De Belizal, E. (2013). Source of the great AD 1257 mystery eruption unveiled, Samalas volcano, Rinjani Volcanic Complex, Indonesia. Proceedings of the National Academy of Sciences, 110(42), 16742-16747.
3. Lazecký, M., Spaans, K., González, P.J., Maghsoudi, Y., Morishita, Y., Albino, F., Elliott, J., Greenall, N., Hatton, E., Hooper, A. and Juncu, D. (2020). LiCSAR: An automatic InSAR tool for measuring and monitoring tectonic and volcanic activity. Remote Sensing, 12(15), p.2430.
4. Ohsawa, S., Saito, T., Yoshikawa, S., Mawatari, H., Yamada, M., Amita, K., Takamatsu, N., Sudo, Y., Kagiyama, T., 2010. Color change of lake water at the active crater lake of Aso volcano, Yudamari, Japan: is it in response to change in water quality induced by volcanic activity? Limnology 11, 207-215.
5. Morishita, Y., Lazecky, M., Wright, T. J., Weiss, J. R., Elliott, J. R., & Hooper, A. (2020). LiCSBAS: An open-source InSAR time series analysis package integrated with the LiCSAR automated Sentinel-1 InSAR processor. *Remote Sensing*, *12*(3), 424.
6. Lazecky, M., Fang, J., Hooper, A., & Wright, T. (2022, July). Improved phase unwrapping algorithm based on standard methods. In *IGARSS 2022-2022 IEEE International Geoscience and Remote Sensing Symposium* (pp. 743-746). IEEE.
7. Lazecký, M., Ou, Q., Shen, L., McGrath, J., Payne, J., Espín, P., Hooper, A. and Wright, T., 2024. Strategies for improving and correcting unwrapped interferograms implemented in LiCSBAS. Procedia Computer Science, 239, pp.2408-2412.
8. Ghorbani, Z., Khosravi, A., Maghsoudi, Y., Mojtahedi, F. F., Javadnia, E., & Nazari, A. (2022). Use of InSAR data for measuring land subsidence induced by groundwater withdrawal and climate change in Ardabil Plain, Iran. *Scientific Reports*, *12*(1), 13998.
9. Van der Woerd, H.J.; Wernand, M.R. Hue-Angle Product for Low to Medium Spatial Resolution Optical Satellite Sensors. Remote Sens. **2018**, 10, 180.
10. Jin, C., Kim, M., Kim, C., Lee, Y., Lee, K. D., Ryu, J. H., & Choi, C. (2023). Accuracy evaluation of reflectance, normalized difference vegetation index, and normalized difference water index using corrected unmanned aerial vehicle multispectral images by bidirectional reflectance distribution function and solar irradiance. *Journal of Applied Remote Sensing*, *17*(4), 044512-044512.
11. Ju, J., Zhou, Q., Freitag, B., Roy, D.P., Zhang, H.K., Sridhar, M., Mandel, J., Arab, S., Schmidt, G., Crawford, C.J. and Gascon, F. (2025). The Harmonized Landsat and Sentinel-2 version 2.0 surface reflectance dataset. *Remote Sensing of Environment*, *324*, p.114723.
12. Grandin, R., Boichu, M., Mathurin, T., & Pascal, N. (2024). Automatic estimation of daily volcanic sulfur dioxide gas flux from TROPOMI satellite observations: Application to Etna and Piton de la Fournaise. *Journal of Geophysical Research: Solid Earth*, *129*(6), e2024JB029309.